Properties of ice cloud over Beijing from surface Ka-band radar observations during 2014–2017

Juan Huo, Yufang Tian, Xue Wu, Congzheng Han, Bo Liu, Yongheng Bi, Shu Duan and Daren Lyu

Key Laboratory for Atmosphere and Global Environment Observation, Chinese Academy of Sciences

Correspondence to: Juan Huo (huojuan@iap.ac.cn)

Abstract. The physical properties and radiative role of ice clouds remain one of the uncertainties in the Earth–atmosphere system. In this study, we present a detailed analysis of ice cloud properties based on four years of surface millimetre-wavelength radar measurements in Beijing, China, where summer monsoon from the ocean and winter monsoon from the continent prevails alternately, resulting in various ice clouds. More than 6300 ice cloud clusters were studied to quantify the properties of ice clouds, such as the height, optical depth and horizontal extent, which can serve as a reference for parameterization and characterization in global climate models. In addition, comparison between ice cloud clusters formed under summer monsoon and winter monsoon indicates the different formation and evolution mechanisms of cirrus. Statistically, temperatures of more than 95% of ice radar bins are below −15°C and more than 80% of ice clouds are above 7 km. The dependence of the radar reflectivity of ice particles on the height and temperature was also observed in this study, indicating that the reflectivity of ice bins increases (decreases) as the temperature (height) increases. In addition, it is found that there is a strong linear relationship between the mean reflectivity and the ice cloud depth. Due to various synoptic circumstances, the ice clouds in summer are warmer, higher, and thicker, with larger reflectivity than that in winter; in particular, the mean cloud-top height of ice clouds in summer is 2.2 km higher than that in winter. Our analysis indicates that most cirrus clouds are of the *in situ*-origin type in winter and autumn; the *in situ*-origin type cirrus clouds are more common than liquid-origin cirrus clouds in spring, while summer features more liquid-origin cirrus clouds.

1. Introduction

The radiative role of ice clouds in the Earth–atmosphere system is known to be significant; however, uncertainties remain in respect of the net effects since ice clouds contain various types of non-spherical ice crystals (Yang et al., 2015). For example, ice clouds absorb the outgoing infrared radiation from Earth's surface and lower atmosphere while reflecting a portion of the incident sunlight back to outer space. When ice clouds are thin enough that the sun can be seen through them, the net impact on the planetary radiation balance is generally one of warming; thicker ice clouds reflect more sunlight and generally result in net cooling (Heymsfield et al., 2017；Kärcher 2018；Kox et al., 2014). Cirrus clouds are dominated by ice crystals. Studies show that the occurrence frequency of the cirrus clouds exhibits latitudinal variability ranging from 50% in the equatorial regions of Africa to 7% in the polar regions (Stubenrauch et al., 2006；Hahn and Warren, 2007；Sassen et al., 2008, 2009).

Ice clouds cover over 50% of the globe's surface (Hong and Liu, 2015). Dolinar et al. (2019) reported that single-layer ice clouds have a global occurrence frequency of about 18%. Ice clouds are an important component of the planetary radiation budget in terms of magnitude; plus, they influence hydrological and climate sensitivities and affect surface climate (Runheng and Liou, 1985; Yang et al., 2015; Gultepe and Heymsfield, 2016; Lawson et al., 2019).

The physical and optical properties of ice clouds, such as ice crystal size, ice shape, particle concentration, cloud-top height (CTH), and optical depth, are heterogeneously and diversely distributed over the globe (Jensen et al., 1996; Mace et al., 2006; Yang and Fu, 2009; Adhikari et al., 2012; Cotton et al., 2013; Heymsfield et al., 2013; Luebke et al., 2016; Wolf et al., 2018; Ge et al., 2019). Recent studies show that cirrus clouds remain one of the largest sources of uncertainty in global climate models (GCMs), due to the deficiencies in representing their observed spatial and temporal variability (Zelinka et al., 2012; Joos et al., 2014; Muhlbauer et al., 2014). According to the IPCC (Boucher et al., 2013), "Especially for ice clouds, and for interactions between aerosols and clouds, our understanding of the basic micro-scale physics is not yet adequate, although it is improving." Understanding the microphysical and macrophysical properties of ice clouds, as well as their relationships with atmospheric states, such as temperature, wind velocity and relative humidity, is important for advancing our fundamental understanding of the formation and life cycles of ice cloud. It is also an essential step toward reducing the uncertainties of estimates of the climatic impact of cirrus and improving the representation of ice clouds in GCMs. A better understanding of ice clouds is important for improving climate simulations and numerical weather predictions.

Millimetre-wavelength radar is a powerful method for observing the macroscopic and microphysical properties of vertical cloud profiles owing to its ability to penetrate the interior of clouds. Because of their short wavelengths, they are sensitive to small cloud droplets and ice crystals, meaning they detect all types of non-precipitating clouds well (Kollias et al., 2007). Radar can perform long continuous observations and the data have high temporal resolution (i.e., detecting three profiles per second with the vertically pointing mode), which is more advantageous than aircraft in understanding the characteristics of daily changes and the formation and development of clouds. Regular calibration for radar can ensure the stability of data and support long-term data for cloud climatology research. This study used long-term, continuous, surface Ka-band radar data to study and understand the microphysical and macrophysical properties of ice clouds over Beijing, China, in the northern mid-latitude region. Beijing (39.96°N, 116.37°E) is in the subtropical monsoon zone with a typical continental monsoon climate. Winds from the southeast ocean prevail in summer while winds from the northwest continent dominate in winter, resulting in hot and rainy summers but cold and dry winters. The formation, evolution and life cycle of ice clouds present regional and distinctive traits, which are created by the regional climate and, to a certain extent, the global climate too. This paper presents the features of ice clouds over mid-latitude monsoon regions through detailed analysis based on long-term radar data, and serves as a reference for cloud parameterization in GCMs.

Section 2 of this paper briefly introduces the Ka-band radar data, the identification method for ice clouds, and other auxiliary datasets. Section 3 describes the macrophysical properties of ice clouds. Details of the microphysical properties of ice clouds are presented in section 4. In section 5, the formation types of cirrus in four seasons are investigated. Conclusions are given in section 6.

2. Data and method

2.1 Ka-band radar

The ice clouds analysed in this study are from observations of a Ka-band polarization Doppler radar (KPDR) situated at the Institute of Atmospheric Physics (IAP; 39.967°N, 116.367°E), Beijing, China. KPDR was set up in 2010 and works at a frequency of 35.075 GHz (wavelength of 8.55 mm) (Huo et al., 2019), measuring the equivalent reflectivity factor (Z_e, hereinafter simply 'reflectivity'; units: mm^6/m^3; dBZ = $10\log(Z_e)$), Doppler velocity, spectral width and linear depolarization ratio of cloud. It is equipped with a Magnetron-type transmitter with a minimum sensitivity of −45 dBZ for cloud determination. For comparison, the 94 GHz cloud profiling radar (CPR) on CloudSat has a sensitivity of approximately −30 dBZ. As shown by *in situ* measurements, the number density of ice particles often peaks at particle sizes between 100 and 1000 μm in effective diameter (Heymsfield et al., 2013). Calculations or measurements of radar reflectivity in previous studies reveal that the reflectivity of ice clouds over mid-latitude regions are mostly larger than −30 dBZ (Deng et al., 2010; Pokharel and Vali, 2011; Matrosov and Heymsfield, 2017). Therefore, KPDR is capable of detecting most ice clouds over Beijing. However, the Ka-band radar is more sensitive to larger particles in a cloud target since the reflectivity is proportional to the D^6 (D is particle size). For the CPR, thin ice clouds with ice water content (IWC) lower than approximately 0.4 mg/m^3 are invisible (Wu et al., 2009). It is possible that KPDR may miss some thin ice clouds when they only consist of very small ice crystals (i.e., D less than 20 μm) or the IWC is smaller than 0.4 mg/m^3. The pulse width of KPDR is 0.2 μs and the beam width is 0.4°. Its repetition frequency is 3.5 KHz and its vertical resolution is 30 m. KPDR has operated daily since 2012, mostly in the vertically pointing mode. During special events—for example, short-term collaborative observations with other instruments—the scanning mode changes to the Plane Position Indicator or Radar Height Indicator mode. In 2013 and 2018, KPDR was non-operational during almost the whole of the summer period. The radar data used in this paper were observed from 1 January 2014 to 31 September 2017. During these four years, the valid operational time of the radar in the vertically pointing mode occupied more than 80% of the total time. Namely, there are more than 28,000 hours of radar measurements in vertically pointing mode during the period 2014–2017.

2.2. Ice and cirrus cloud identification

Ice cloud is composed of various types of ice crystals and is usually thin. Cirrus clouds also consist of ice crystals. Definitions of cirrus clouds in previous publications provide us with references for ice cloud identification with KPDR. For example, in the cloud classification algorithm developed for the CPR on the CloudSat satellite, the average temperature at the largest Z_e, the largest Z_e, the average height of the maximum Z_e, the cloud-base height (CBH), etc., are combined to determine cirrus cloud (Wang and Sassen, 2001b). Sassen et al. (2008) classified cloud layers as cirrus via defining two criteria; namely, the visible optical depth should be less than 3.0 and the cloud-top temperature should be lower than −40°C, categorizing cirrus clouds via cloud physical and optical parameters. Deng et al. (2010) identified cirrus layers by cloud-top and cloud-base temperature ($T_{top} < -40$°C and $T_{base} < -10$°C). In some recent studies, cirrus clouds are defined as ice clouds in the temperature

range < −38°C (Krämer et al., 2016; Luebke et al., 2016; Heymsfield et al., 2017). Ge et al. (2019) used two temperature criteria to identify cirrus cloud: the temperature of the cloud top should be less than −30 °C and the temperature at the maximum Z_e layer and at the cloud base should be less than 0°C. KPDR has a cloud clustering and classification algorithm, a detailed description of which has been presented by Huo et al. (2019). Here, we briefly describe it as follows. Firstly, the KPDR cloud profiles are grouped as clusters based on a combination of a time–height clustering method and a *k*-means clustering method. After each cloud cluster is determined, a fuzzy logic method is applied using multiple cloud properties, such as CBH, cloud depth (CD), radar reflectivity, etc., to classify the cloud cluster into nine types: Cs, Cc, Ac, As, St, Sc, Ns, Cu and Cb clouds. According to the definitions and identification approaches in previous studies, we use two criteria to identify ice clouds from KPDR data after the clustering and classification algorithm is performed. Namely, a cloud cluster for which the mean cloud-top temperature is less than −40°C and the maximum cloud-base temperature is less than −10°C is determined as ice cloud. The ice cloud with cloud-base temperature below −38°C is regarded as cirrus cloud in this paper. It should be noted that supercooled water might exist in ice clouds with temperature above −38°C, and thus what the radar measures should indicate different physical properties from that of ice particles. In this paper, the supercooled water is not distinguished and its proportion and properties will be investigated in the future.

2.3 Other datasets

This study also used some other datasets to complement the investigation of the properties of ice and cirrus cloud, such as the temperature profile, water vapor, wind velocity, and cloud optical thickness. The research datasets of cloud optical thickness (produced from Himawari-8) used in this paper were supplied by the P-Tree System of the Japan Aerospace Exploration Agency (https://www.eorc.jaxa.jp/ptree/index.html; last accessed 6 January 2020). Other meteorological reanalysis data employed were from the European Centre for Medium-Range Weather Forecasts (ECMWF) ERA5 datasets (https://www.ecmwf.int/en/forecasts/datasets/reanalysis-datasets/era5; last access: 6 January 2020).

3. Macrophysical properties

3.1 Ice cloud samples under summer and winter monsoon

Ice clouds can be vertically and horizontally extensive, with their various appearances dependent on the diverse range of associated atmospheric movements and processes. KPDR is located in the north of the North China Plain, where to the west and north there are mountains and to the south and east is the Bohai Sea. In the region's hot summers, monsoon from the sea brings large quantities of water vapour, whereas dry and cold monsoon from the northern continent dominates this region in winter. These different monsoon types support various atmospheric conditions, such as increasing relative humidity, cooling, updrafts, etc., required for the formation of ice clouds, ultimately resulting in distinct cirrus distributions. Figure 1 presents a

typical example of an ice cloud distribution collected by KPDR in one month of winter (January 2016) and one month of summer (August 2015).

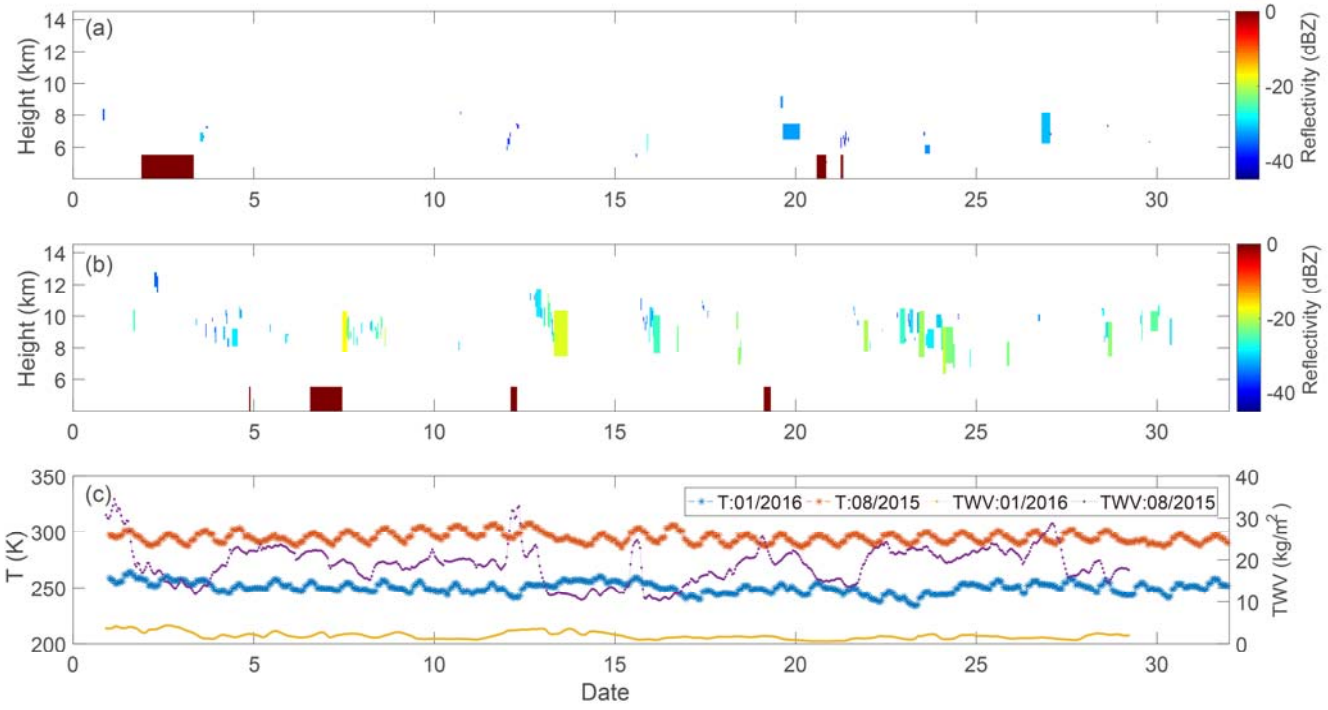

Figure 1. Ice clouds occurring in (a) January 2016 (winter) and (b) August 2015 (summer). The mean cloud-top height, mean base height and lifetime of each ice cluster forms an ice cloud "rectangle". Its mean radar reflectivity is illustrated with different colours. Dark red rectangles on the horizontal axis indicate periods without vertically pointing radar measurements. The surface temperature (T, left-hand *y*-axis) and total water vapour (TWV, right-hand *y*-axis) in the two months are presented in (c).

There are more ice clouds in August than in January, and the mean radar reflectivity of ice cloud in August is higher than that in January. Ice clouds in August also show larger vertical dimensions than in January. The temperature and amount of water vapour are two key parameters in the formation of clouds, especially in plain areas where orographic uplift is negligible. The strong contrast in the climatic circumstances between a month in summer and a month in winter generates a diverse range of ice clouds (Fig. 1c). Thus, to better understand the physical or optical properties of ice clouds, statistical analyses were carried out in this study for different seasons. Such comparisons of the ice clouds among the four seasons benefit our understanding of the dominant formation origins of ice clouds when a region is governed alternately by different monsoon types. In this study, four years of radar observations presented more than 6300 ice cloud clusters for our analysis.

3.2 Monthly and hourly occurrence frequency

Radar data collected in vertically viewing mode were used to calculate the occurrence frequency of all clouds (O_{all}), which is the ratio of cloudy profiles to all profiles in a certain time range (i.e., an hour or a month), as well as the occurrence frequency of ice clouds (O_{ic}), which is the ratio of profiles determined as ice clouds to all radar profiles:

$$O_{all} = N_{all} / N_r, \quad (1)$$

$$O_{ic} = N_{ic} / N_r, \quad (2)$$

where N_{all} is the number of cloudy profiles, N_r is the number of all radar profiles, and N_{ic} is the number of ice cloud profiles. Figure 2 shows the monthly occurrence frequency of all clouds and ice clouds in four years. In addition, the occurrence frequency of cirrus clouds is also presented for contrast. September has the maximum O_{all} among all months, and summer/winter has the maximum/minimum O_{all} among the four seasons. Relative to O_{all}, O_{ic} decreases to 33%–50%, and in winter O_{ic} is about 33% of O_{all}. The average O_{ic} in April and June is about 20%, whereas in winter (December–February) it is no more than 10%. The average O_{ic} in the four years is 14%, which is lower than the ice cloud coverage of 24% reported by Hahn and Warren (2007) based on satellite measurements over North China. This might be associated with the observation location and the field of view (FOV) of the KPDR. Large quantities of water vapour over the sea areas and orographic-lift movements over mountain areas provide advantageous conditions for the formation of clouds, meaning more clouds occur over these areas relative to plain areas. Therefore, the occurrence frequency calculated from the KPDR data with a small FOV are lower than the cloud coverage calculated from data with a broad FOV. For cirrus clouds, the largest occurrence frequency (4%) occurs in April. Spring but not summer has the most cirrus clouds.

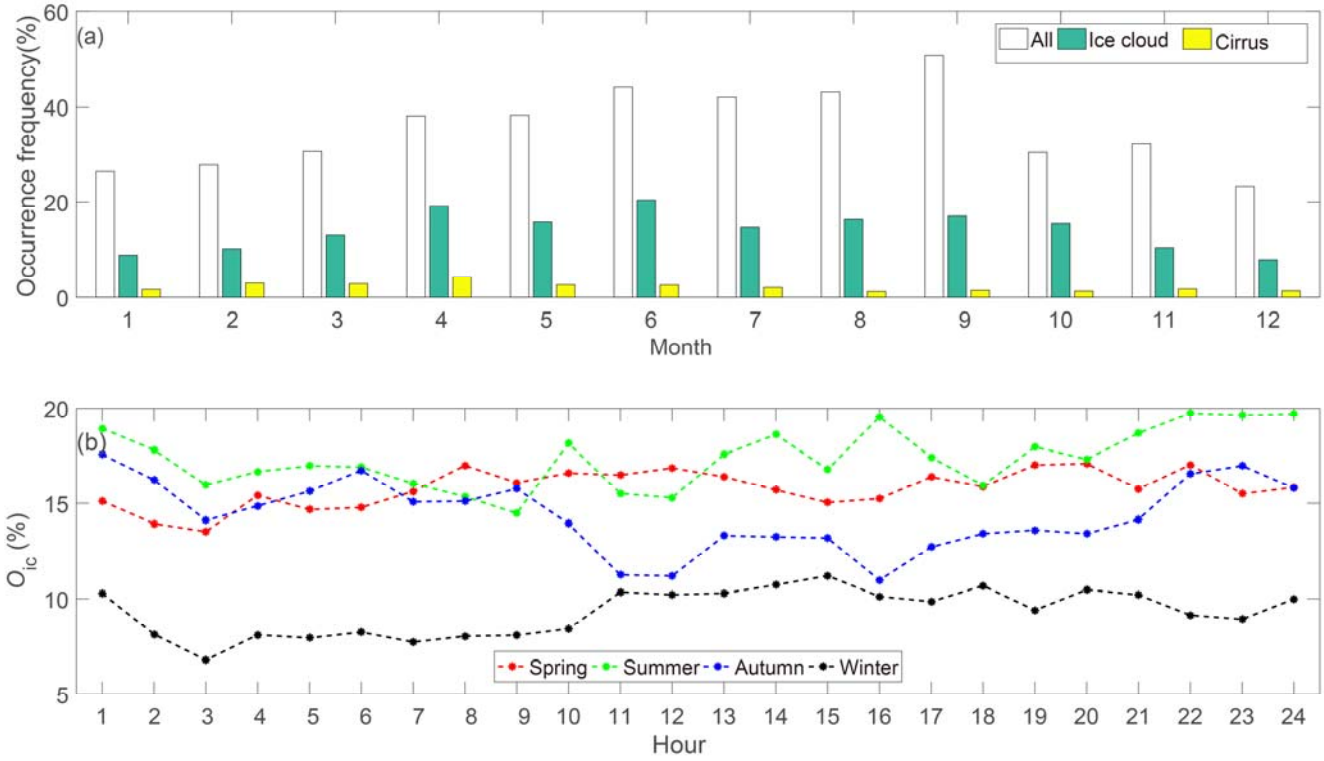

Figure 2. Monthly occurrence frequencies of all clouds (O_{all}), ice clouds (O_{ic}) and cirrus clouds (a), along with the diurnal O_{ic} in the four seasons (b).

KPDR operates continuously and thus allows the diurnal variation of O_{ic} to be studied, which illustrates the potential relationship with local thermal convection caused by solar heating. As shown in Fig. 2a, the three highest O_{ic} values in spring, summer, autumn and winter occur at 20:00/22:00/19:00, 21:00/23:00/22:00, 00:00/22:00/21:00 and 14:00/13:00/17:00, respectively. The hourly variations of O_{ic} in the four seasons are different; in spring, summer and autumn, larger O_{ic} values appear at night, whereas larger O_{ic} values in winter appear during daytime. The diurnal variation of O_{ic} seems to be insensitive to solar heating, which drives the development of regional thermal convection. Here, the presence of ice clouds over KPDR is not closely related with local air-updraft activities, indicating that these ice clouds mostly may not be generated locally by thermal convections. It is interesting that O_{ic} decreases from 00:00 to 02:00 and then increases after that in the four seasons. Is there a decay process in ice clouds during this period? Is the decrease caused by wind, vertical movement or turbulence? Further analysis is required in the future to answer these questions.

3.3 Height, depth and extent

The top height of ice cloud, especially cirrus cloud, indicates the highest condensation level in the troposphere, above which clouds cannot form because of the non-conducive condensation conditions. The base height of ice clouds indicates the lowest level required for ice formation. In this study, the CTH and CBH were calculated for each ice cloud cluster; specifically, the CTH and CBH are the mean values of all cloudy profiles in an ice cloud cluster. The distributions of the mean CTH and CBH of all ice clouds in the four seasons are presented in Fig. 3, and Table 1 presents the quantified statistical results.

It is shown that the CTH of ice clouds varies in the range of 5.5–12.9 km (Fig. 3a). The difference between the maximum and the minimum is about 6 km in each season, indicating the ranges of the condensation level and various formation mechanisms of ice clouds. Besides, differences in the CTH between the four seasons are also apparent. Both the maximum (12.9 km) and the highest mean CTH (9.27 km) are found in summer, whereas winter has the minimum CTH (9.94 km) and lowest mean CTH (7.02 km). In summer, 85% of ice clouds have a CTH greater than 8 km and 29% are greater than 10 km. In winter, 71% of ice clouds have a CTH larger than 8 km, and those with a CTH higher than 6 km account for 97%. The mean CTH in summer is 2.2 km higher than that in winter, which means the average condensation level in summer is also 2.2 km higher. Spring and autumn are two transition seasons and their CTHs are 8.16 km and 8.23 km, respectively, which are between those of summer and winter.

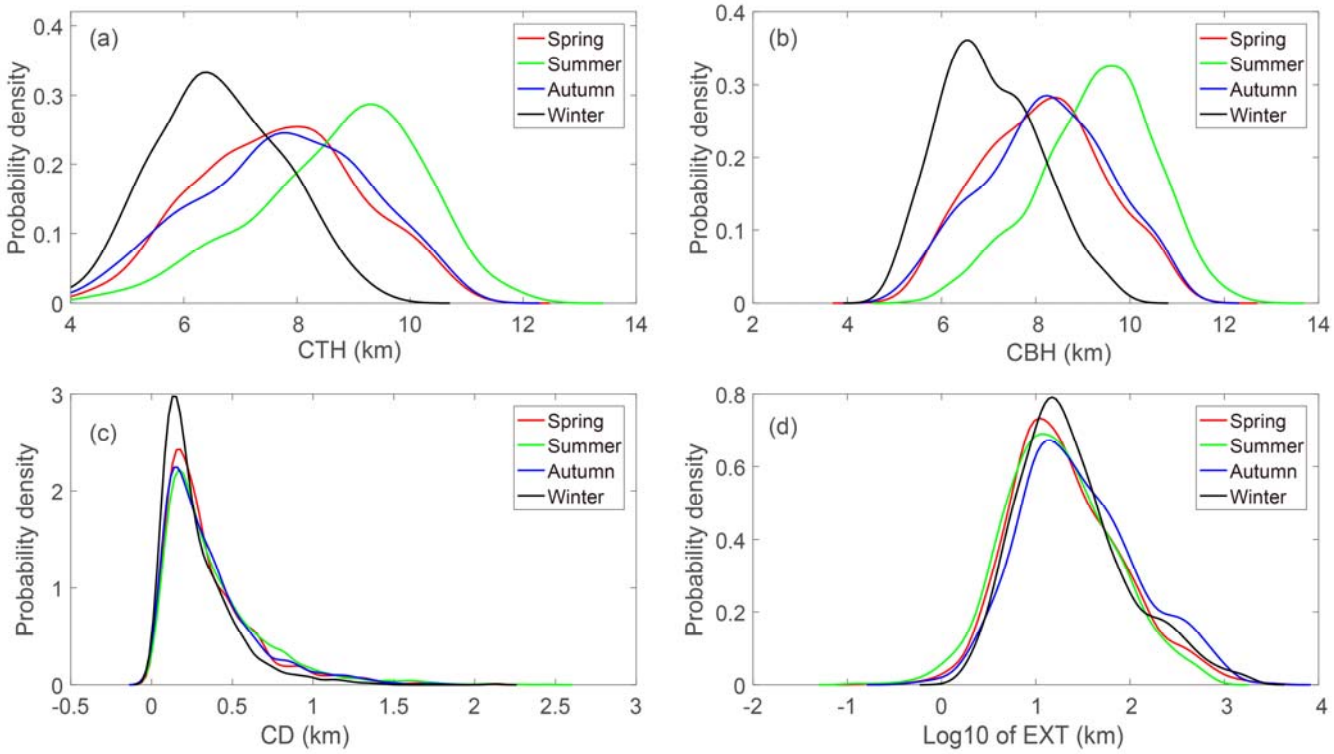

Figure 3. Distribution of cloud-top height (a), cloud-base height (b), cloud depth (c), and horizontal extent (EXT) (d) in the four seasons. In (d), EXT is shown as log10 values.

Figure 3b shows that the CBH changes within a range of 5.3–12.4 km, and the minimum CBHs in the four seasons are close to each other, ranging between 5.3 and 5.7 km. However, the mean CBH in summer is the highest (8.7 km) among the four seasons, while the lowest (6.6 km) is in winter. The difference in CBH between summer and winter is 2.1 km. The mean CBHs in spring and autumn are both 7.7 km. In summer, the percentage of ice clouds with a CBH larger than 8 km is 72%, while it is only 65% in winter. In summer and winter, 95% of ice clouds have a CBH greater than 6 km.

It is shown that the mean CDs of ice clouds in the four seasons are close, with the depths of most clusters being less than 1 km (Fig. 3c). Statistically, in the four seasons, 68% of clusters have a CD of less than 0.5 km, 90% less than 1 km, and 96% less than 1.5 km. It should be noted that the CTH, CBH and CD here are the mean values of an ice cloud cluster. It is therefore possible that there are some instances of CTH, CBH and CD that are greater than their corresponding mean values.

The horizontal extent (EXT) of ice clouds indicates its lifetime and the formation mechanism type. For the KPDR, the EXT of an ice cloud cluster is computed as follows:

$$\mathrm{EXT} = V_{\mathrm{hw}} \times T_{\mathrm{ci}}, \quad (3)$$

where V_{hw} is the mean velocity of horizontal wind calculated from the ECMWF-ERA5 dataset and T_{ci} is the continuous time during which an ice cluster moves over the KPDR. It is found that the maximum EXT of ice clouds reaches 2800 km, which is in April 2017, and the maximum T_{ci} is 21 hours, which is in March 2016. The EXT ranges through orders of magnitude from

low values of less than 0.1 km to over 2800 km. Summer has the minimum mean, median and trimmed mean EXT, while ice clouds in autumn have the maximum mean, median and trimmed mean EXT. Statistically, about 75% of ice clouds have an EXT less than 50 km and 87% less than 100 km. The statistically quantified structural properties of ice clouds in the four seasons are presented in Table 1.

Table 1. Statistical results for the cloud-top height (CTH), cloud-base height (CBH), cloud depth (CD) and horizontal extent (EXT) in the four seasons. The 'trimmean' is the 10% trimmed mean of portion clusters, excluding 10% of clusters with the highest and lowest values (unit: km).

Season	Parameters	Mean	Median	Trimmean	Maximum	Minimum
Spring	CTH	8.16	8.17	8.15	11.74	5.73
	CBH	7.68	7.68	7.68	11.43	5.43
	CD	0.35	0.27	0.32	2.1	0.06
	EXT	61.5	17.34	35.6	2824.9	0.18
	COD	4.27	3.22	3.81	–	0.06
Summer	CTH	9.27	9.38	9.30	12.86	6.10
	CBH	8.73	8.97	8.78	12.42	5.64
	CD	0.39	0.30	0.35	2.45	0.06
	EXT	43.0	16.1	29.6	725.1	0.13
	COD	6.07	4.28	5.64	–	0.1
Autumn	CTH	8.23	8.27	8.24	11.25	5.69
	CBH	7.74	7.80	7.77	11.07	5.31
	CD	0.35	0.28	0.33	1.82	0.06
	EXT	86.10	23.5	55.17	2863.8	0.47
	COD	4.62	3.05	4.01	–	0.01
Winter	CTH	7.02	6.90	7.00	9.94	5.50
	CBH	6.63	6.57	6.63	9.75	5.30
	CD	0.28	0.21	0.26	2.13	0.04
	EXT	72.7	19.3	41.4	1695.2	1.50
	COD	4.52	2.80	4.10	–	0.21

3.4 Optical depth

Cloud optical depth (COD) is relatively independent of wavelength throughout the visible spectrum. In the visible portion of the spectrum, the COD is almost entirely due to scattering by droplets or crystals of clouds (American Meteorological Society, 2019). Therefore, the CODs of ice clouds depend directly on the CD, the IWC, and the size distribution of the ice crystals, indicating a cooling effect or warming effect in the energy budget.

The Advanced Himawari Imager (AHI), onboard the geostationary meteorological Himawari-8 satellite operated by the Japanese Meteorological Agency, observes the Beijing area every 10 min and began releasing COD and cloud-type products

in July 2015 with a spatial resolution of 5 km. The CODs are retrieved by using non-absorbing visible wavelengths (i.e., 0.51 or 0.64 μm) and water-absorbing, near-infrared wavelengths (i.e., 1.6 or 2.3 μm) (Nakajima and Nakajma, 1995; Kawamoto et al., 2001). Quantified uncertainties of the AHI-CODs have not been reported, so we use them here directly. The data nearest to KPDR that AHI determine as cirrus cloud and KPDR determine as ice cloud are selected and their CODs are investigated. Those collocated CODs (collected from the year 2016 to 2017) combined with the mean CDs and mean reflectivity, which are calculated from all cloudy KPDR bins observed within 10 min of the AHI observing time, are presented in Fig. 4.

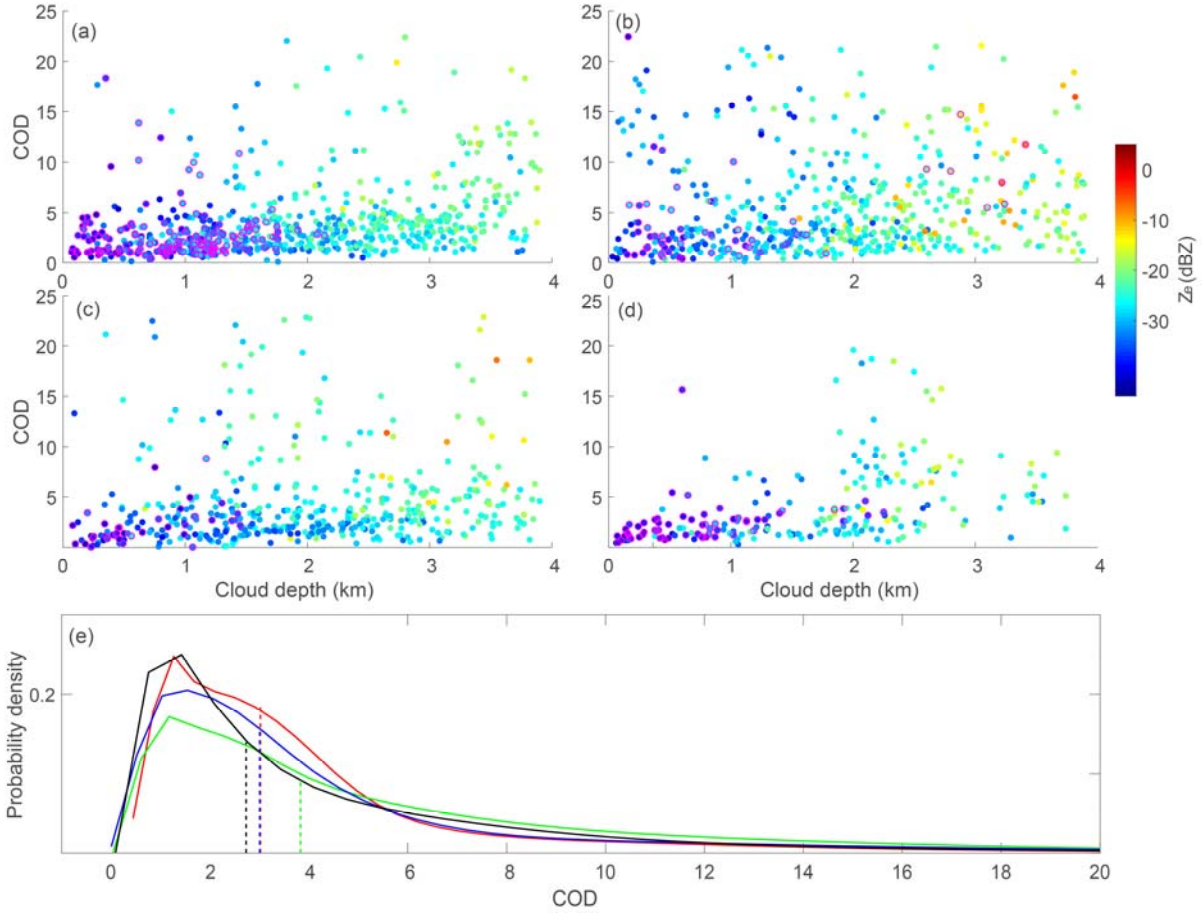

Figure 4. The cloud optical depth (COD) of ice clouds in terms of the cloud depth in spring (a), summer (b), autumn (c), and winter (d). Colors indicate the mean reflectivity of those radar profiles within 10 min of the AHI (Advanced Himawari Imager) observation time. Cases with cloud-base temperatures lower than −38°C are illustrated with purple edges. Panel (e) presents the probability density distribution of the COD in the four seasons.

In the four seasons, CODs show an increasing tendency with increasing CD. The mean reflectivity shows a similar tendency, meaning thicker ice clouds generally contain larger particles and a greater number density of ice particles. The probability density distributions of COD in the four seasons show a higher probability occurring at lower COD. The mean COD in spring, summer, autumn and winter is 4.27, 6.07, 4.62, and 4.52, respectively. The proportions of CODs lower than 3 in spring, summer, autumn and winter are 46%, 36%, 49% and 52%, respectively. The proportions of CODs lower than 10 in

the four seasons are 91%, 79%, 87% and 90%, respectively. In Fig. 4, KPDR cirrus clouds are shown with purple circles. The proportions of CODs for cirrus clouds lower than 3 in spring, summer, autumn and winter are 70%, 55%, 77% and 79%, respectively. The proportions of CODs lower than 6 in the four seasons are 93%, 77%, 94% and 98%, respectively. As shown in previous studies, the primary cirrus optical depth is below 3 (Kienast-Sjögren et al., 2016; Sassen et al., 2008). Here, our analysis shows larger COD, indicating possible mixed-phase clouds. Also, it might be related with the uncertainty in CODs, as the uncertainties of AHI-CODs and the different FOV between KPDR and AHI may cause the employed CODs to differ from the real CODs. The results here present statistical features of the COD of ice clouds over Beijing based on a COD dataset of limited accessibility. For cirrus clouds, lidar should provide accurate COD measurements.

4. Microphysical properties

The most important microphysical quantities of ice clouds are the ice particle size distribution, the IWC, and their shapes (Heymsfield et al., 2017). It is known that the radar equivalent (or effective) reflectivity factor can be expressed as

$$Z_e=\frac{\lambda^4}{\pi^5}\left|\frac{m^2-1}{m^2+2}\right|^{-2}\iiint \sigma(D,\theta,\Phi)N(D,\theta,\Phi)\mathrm{d}D\mathrm{d}\theta\mathrm{d}\Phi, \quad (4)$$

where $\sigma(D,\theta,\emptyset)$ is the backscattering cross section with maximum dimension D and an axial direction $(\theta,\emptyset)$ with respect to the radar beam, $N(D,\theta,\emptyset)$ is the number density, λ is the wavelength, and m is the complex index of refraction of the scattering target. To date, numerous empirical relationships between Z_e and cloud properties (P)—e.g., IWC, snow precipitation rate—have been developed, usually in the power-law form of

$$Z_e = AP^B, \quad (5)$$

where A is the prefactor coefficient and B is the exponent derived in terms of calculated or measured datasets (Liu and Illingworth, 2000; Wang and Sassen, 2001a; Heymsfield et al., 2008; Austin et al., 2009; Delanoë and Hogan, 2010; Deng et al., 2015; Matrosov and Heymsfield, 2017; Heymsfield et al., 2018). Delanoë and Hogan (2008, 2010) proposed a different method using a forward model to retrieve the IWC and the effective radius by combination with the COD. Also, the basic principles of this method are applied in the CloudSat/CALIPSO cloud microphysical retrieval algorithm. However, the use of empirical relations such as Eq. (5) is still common in many practical measurements, and the correspondence between the IWC and Z_e is related with the particle size distribution (the gamma distribution is mostly used for ice clouds).

For the KPDR, the development of the IWC and particle size retrieval algorithm is in progress but has not been tested completely. In this paper, we use the measured radar reflectivity factor Z_e directly, not the retrieved microphysical quantities, to study and characterize the microphysical properties of ice clouds. It can be found from Eq. (4) that reflectivity increases when σ and N increase; in other words, a larger reflectivity normally indicates a larger D, N and IWC.

4.1 Reflectivity and height dependence

KPDR detects clouds at a 30 m vertical resolution. All ice radar bins collected from 2014 to 2017 were counted according to their reflectivity and height, and the relative frequencies (counts; calculated at 0.25 dBZ and 30 m interval) are shown

separately in Fig. 5. In summer, the reflectivity mostly varies between −35 and −10 dBZ, while most of the reflectivity falls within the range of −40 to −20 dBZ in winter. In spring and autumn, the reflectivity primarily ranges between −35 and −15 dBZ. The range of variation in reflectivity in summer is the biggest among the four seasons, while it is smallest in winter. Statistically, at the same height where ice clouds exist in the four seasons, the mean reflectivity of winter is 5 dBZ less than that of spring or autumn, and it is 10 dBZ less than that of summer. In the four seasons, the mean reflectivity declines as the height increases, with a similar slope. It can also be seen that the ice bins in summer are located at higher heights than in winter.

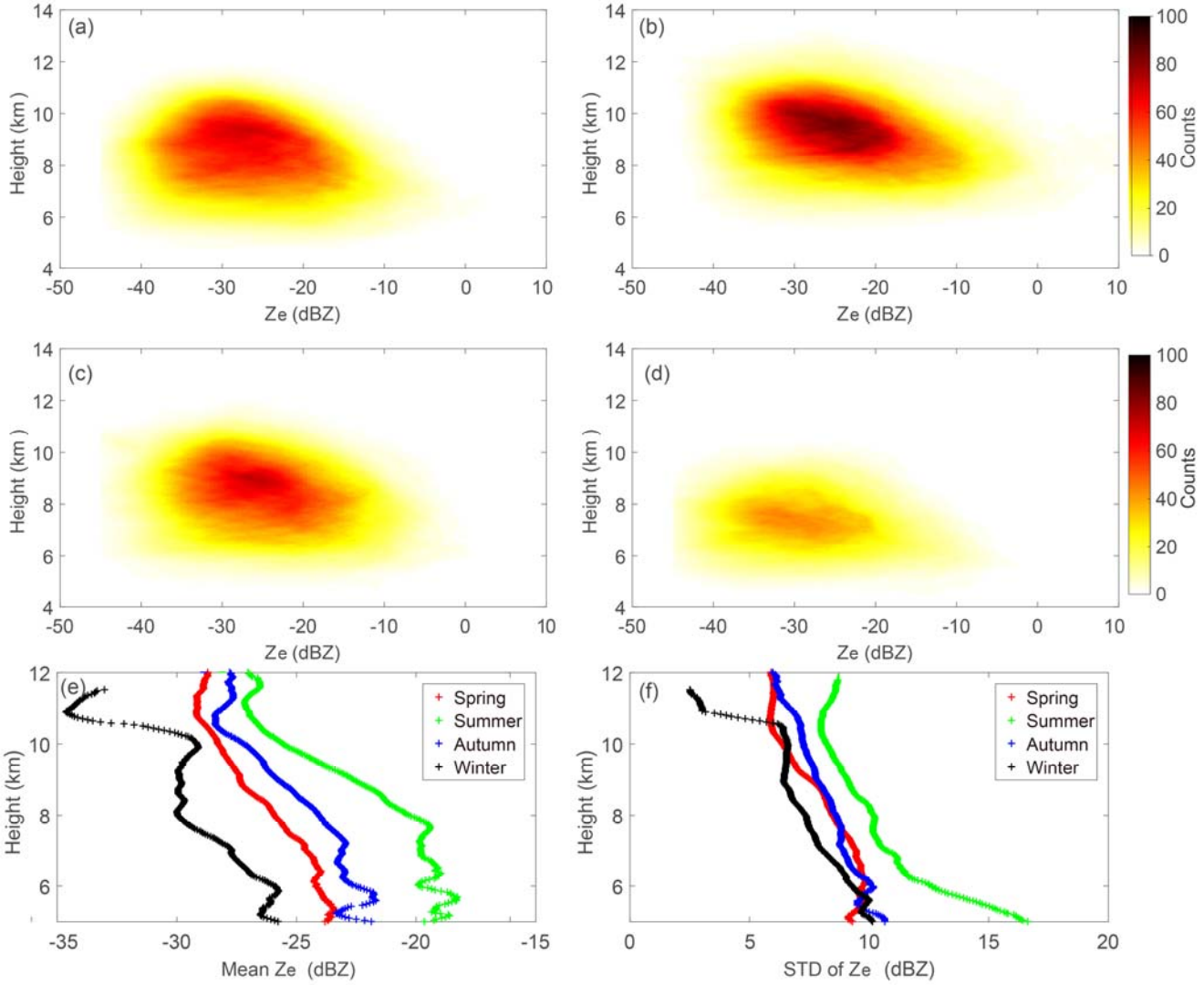

Figure 5. The frequency of reflectivity versus height in spring (a), summer (b), autumn (c) and winter (d). Colors are the values of the counts divided by 1000 (calculated at 0.25 dBZ and 30 m intervals). The mean reflectivity calculated at various heights and the corresponding standard deviation (STD) are presented in (e) and (f), respectively.

4.2 Temperature dependence

Temperature plays a key role in the formation, evolution and lifetime of ice clouds. Activation of liquid waterdrops does not happen below −38°C because the relative humidity where the ice forms is below water saturation. At temperatures higher than −38°C, primary ice clouds form only when aided by ice nucleating particles (Kanji et al., 2017). The summer monsoon and winter monsoon in Beijing support distinct temperatures, water vapor, etc., i.e., the conditions necessary for the formation of ice clouds, resulting in distributions of reflectivity with different features corresponding to temperature. The frequencies (counts; calculated at 0.25 dBZ and 1 °C interval) are shown separately in Fig. 6.

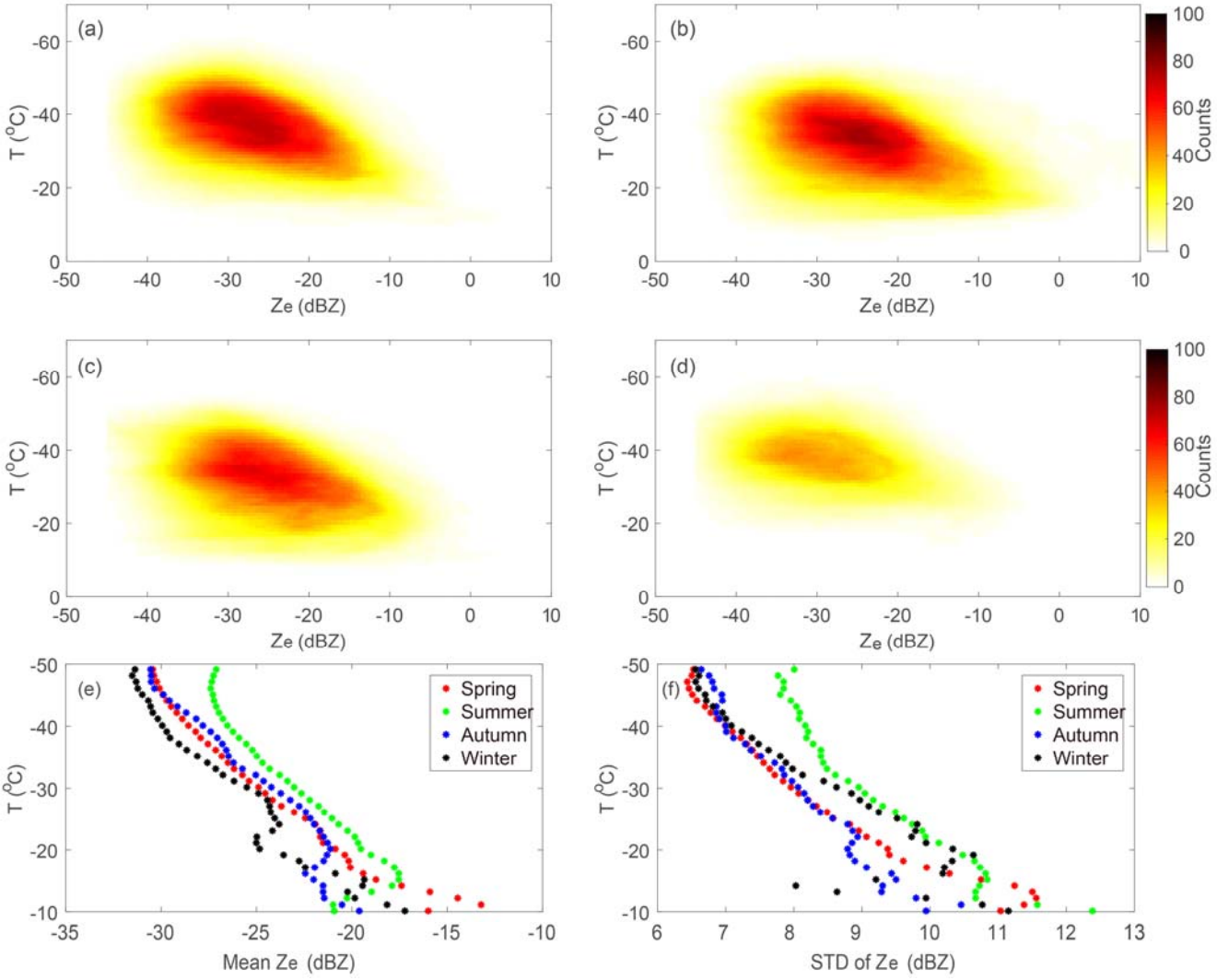

Figure 6. As in Fig. 5 but for temperature, and the colors are the values of the counts (calculated at 0.25 dBZ and 1°C intervals) divided by 5000.

In spring, summer and autumn, ice clouds occur mostly at temperatures within the range of −20°C to −45°C, relative to which ice clouds in winter occur at lower temperatures. It should be noted that, due to the very wide variation range, very small counts are also displayed in Fig. 6 but are hard to distinguish since they are closer to zero. Statistically, the percent of ice bins with temperatures less than −15°C is 99%, 95%, 95% and 99% in spring, summer, autumn and winter, respectively; the percent of ice bins with temperatures less than −25°C is 85%, 71%, 72% and 92% in spring, summer, autumn and winter, respectively; and the percent of ice bins with temperatures less than −35°C is 52%, 36%, 35% and 60% in spring, summer, autumn and winter, respectively. The reflectivity shows a dependence on the temperature, increasing when temperature increases. Statistically, the mean temperature of ice clouds in winter is lower than that in other seasons, even though these ice clouds appear at lower heights. As the temperature decreases, the difference in reflectivity between winter and summer declines. At the same temperature, the mean reflectivity in summer is higher than that in winter. The slopes among the four seasons are close to each other, demonstrating a determinative effect of the temperature on the cloud particle properties.

4.3 Depth dependence

Based on all the ice clusters in the four years, we calculated the mean reflectivity and the mean depth of each cluster (Fig. 7), and it was interesting to find that there is a strong linear relationship between the mean reflectivity and the CD. Specifically, the mean reflectivity increases as the CD increases. The linear equation shown in Fig. 7 represents a method that can be used to estimate the mean reflectivity (or CD) if the CD (or reflectivity) is known, which should be useful for cloud parameterization in GCMs.

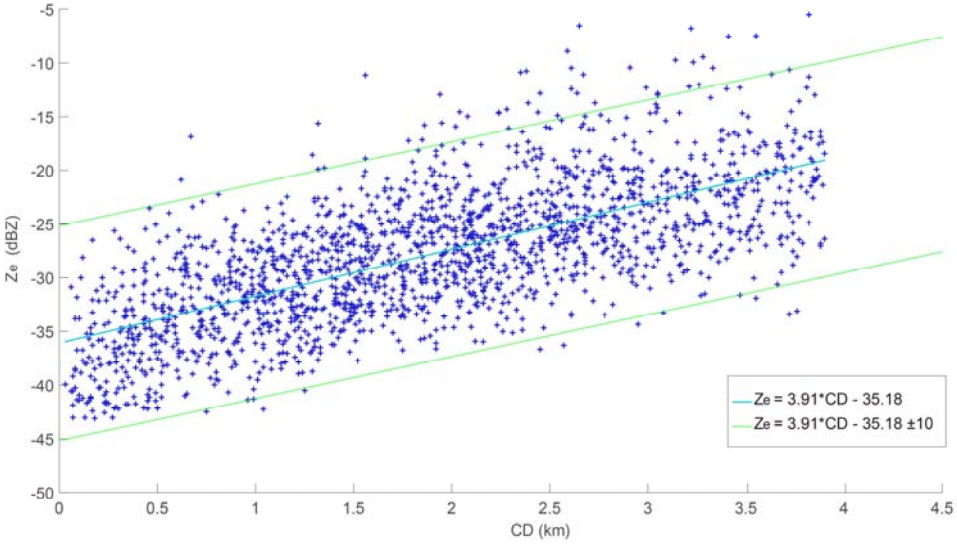

Figure 7. The mean reflectivity of ice clouds as a function of cloud depth (CD).

5. Origination type of cirrus clouds

Kramer et al. (2016) and Luebke et al. (2016) classified two types of cirrus cloud according to their formation mechanism; namely, *in situ*- and liquid-origin cirrus cloud. The *in situ*-origin cirrus type forms directly as cirrus, while the liquid-origin type originates from mixed-phase clouds that are completely frozen until they are lifted to temperatures of < −38°C. They reported that the *in situ*-origin cirrus are mostly thin, with lower IWC, while liquid-origin cirrus tend to be thicker with higher IWC. Also, liquid-origin cirrus tends to have larger ice crystals than *in situ*-origin cirrus. Various prefactor coefficients dependent on temperature have been derived and applied in the Z_e–IWC power-law relationship [i.e., Eq. (5)] since the distribution of reflectivity has a dependence on temperature, just as shown above in section 4.2 (Hogan et al., 2006; Heymsfield et al., 2013; Matrosov and Heymsfield, 2017; Heymsfield et al., 2018). Therefore, the reflectivity of *in situ*-origin cirrus should generally be less than that of liquid-origin cirrus.

In this section, based on the frequency statistics in section 4.2, we calculated the distribution of reflectivity (similar to the probability density function, PDF) at several temperatures to investigate the origin type of cirrus in Beijing. Figures 8–11 show the normalized frequency of reflectivity at central temperatures of −65°C, −60°C, −55°C, −50°C, −45°C and −40°C within ±1°C in spring, summer, autumn and winter, respectively. The maximum counts 'n' used to normalize the frequency is also presented in the figures.

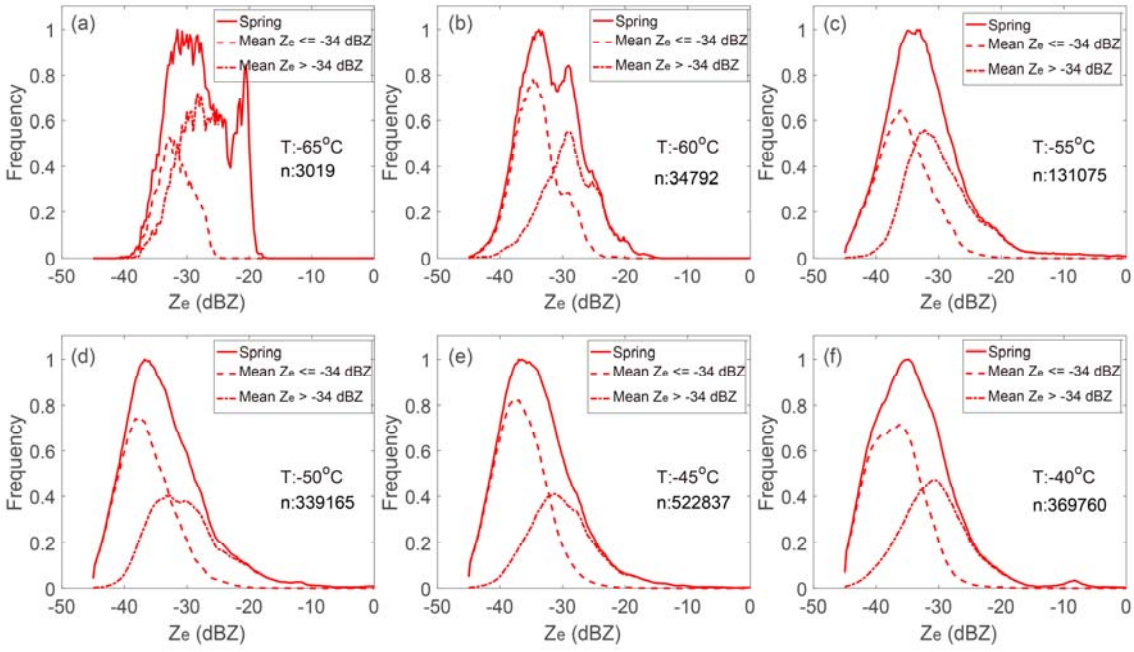

Figure 8. Normalized frequency of the reflectivity at different temperatures (T) in spring. The solid line is the frequency calculated from all cirrus. The dashed line is the frequency calculated from cirrus with a mean Z_e < −34 dBZ. The dash-dotted line is the frequency calculated from cirrus with a mean Z_e above −34 dBZ. The dashed line corresponds to the *in situ*-origin type and the dotted line to the liquid-origin type. The 'n' is the maximum number used to normalize the frequency.

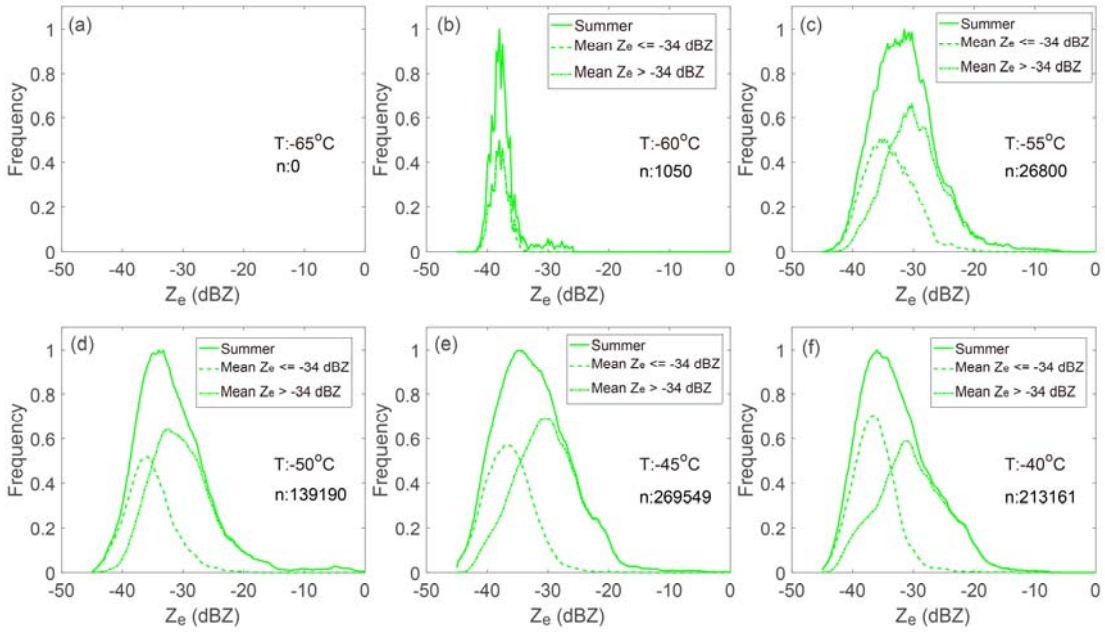

Figure 9. As in Fig. 8 but for summer. No cirrus is found when temperature is at or below −65°C in summer.

Cirrus clouds present diverse reflectivity frequency distributions in terms of temperature in the four seasons. There is no cirrus cloud detected in summer and autumn (see Fig. 9a and Fig. 10a) at or below −65°C. The number of cirrus cloud bins at −65°C in spring and autumn is very small when compared to other temperatures above −50°C. This might be because the frequency of atmospheric temperature < −65°C within the troposphere over Beijing is small, so cirrus clouds at and below this temperature are few. Cirrus clouds also occur little in summer and autumn at −60°C, due to the higher average temperature than in the other two seasons. Above −55°C, the peak frequency center in winter locates at a smaller reflectivity value than that in summer, indicating smaller particles and number density than in summer. In the four seasons, the 'n' at −45°C is the biggest among all temperatures, indicating that cirrus cloud appears more frequently at −45°C than at other temperatures. This is the result of the combination of temperature, water vapor and upward movement. For example, the lower the temperature, the more conducive it is to the formation of ice particles. On the other hand, limited upward movements determine the maximum height (lowest temperature) where water vapor or cloud particles can reach. Spring has the biggest 'n' at each temperature, indicating that cirrus clouds in spring are the most frequent, which has also been shown in Fig. 2.

A bimodal PDF is found at some temperatures—for example, at −60°C and −65°C in spring and at −45°C in autumn. However, most PDFs show a unimodal feature. One possibility is that only one origin type exists in Beijing. Another possibility is that difference between the two origin types is not clearly distinguished. It might be related with the measurement specialties of radar since the Z_e indicates the backscattering from numerous particles and the Z_e is more sensitive to the larger particles in a cloud target.

We divided cirrus clouds into two groups using mean-Z_e threshold to study whether cirrus clouds over Beijing also originate from different mechanisms. If the PDFs of the two separate groups exhibit distinct features, it is possible that they form from different mechanisms. It is found that the cirrus clouds in spring and summer (Fig. 8 and Fig. 9) can be separated clearly into two groups by a threshold of −34 dBZ, and the two groups demonstrate different PDFs after attempting each threshold between −32 dBZ and −38 dBZ. The full width at half maxima and the peak center are different. In addition, the proportions of the two groups are comparable. However, in autumn and winter, cirrus clusters with mean reflectivity less than −34 dBZ contribute the absolute majority of all cirrus clusters when compared with the cirrus with reflectivity larger than −34 dBZ, illustrating different PDFs with those in spring and summer. It is possible that the differences in the PDF among the four seasons is due to the different origin type. For a mean $Z_e \leq -34$ dBZ, cirrus cloud is likely to be an *in situ*-origin cirrus; for a mean $Z_e > -34$ dBZ, cirrus cloud is likely to be a liquid-origin cirrus. From Fig. 8 and Fig. 9, it can be seen that spring has more *in situ*-origin cirrus, while summer has more liquid-origin cirrus. In winter and autumn, cirrus with a mean $Z_e \leq -34$ dBZ dominates, which means that the dominant cirrus in winter and autumn are *in situ*-origin cirrus. Summer has more convective movements and water vapor resulting in dominant liquid-origin cirrus.

As mentioned above, there might be another possibility that only one origin type dominates over Beijing, since most PDFs are unimodal. Large-scale synoptic and dynamic analysis should be carried out to distinguish the dominant origin type. At present, however, we prefer the view that there are two origin types in Beijing, since they are consistent with the basic weather characteristics in the four seasons. Nonetheless, more work will be performed in the future to confirm the current assumptions. On the whole, the formation mechanisms of cirrus in spring and summer in Beijing illustrate different features to those in autumn and winter. It can also be found that the distribution of reflectivity depends not only on the temperature but also on the origin type.

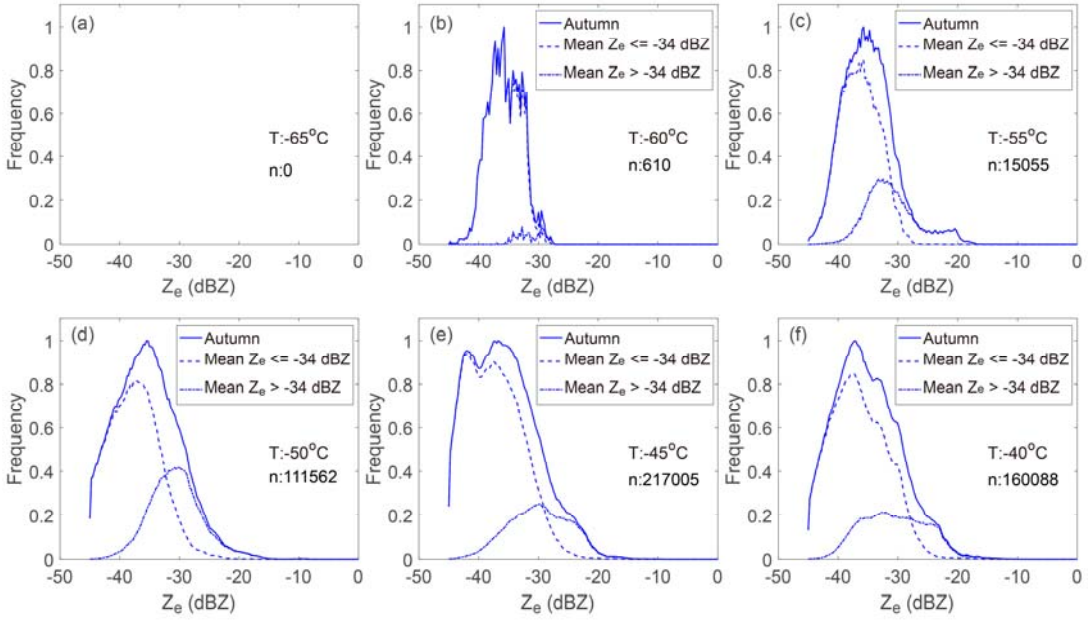

Figure 10. As in Fig. 8 but for autumn. No cirrus is found when the temperature is at or below −65°C in autumn.

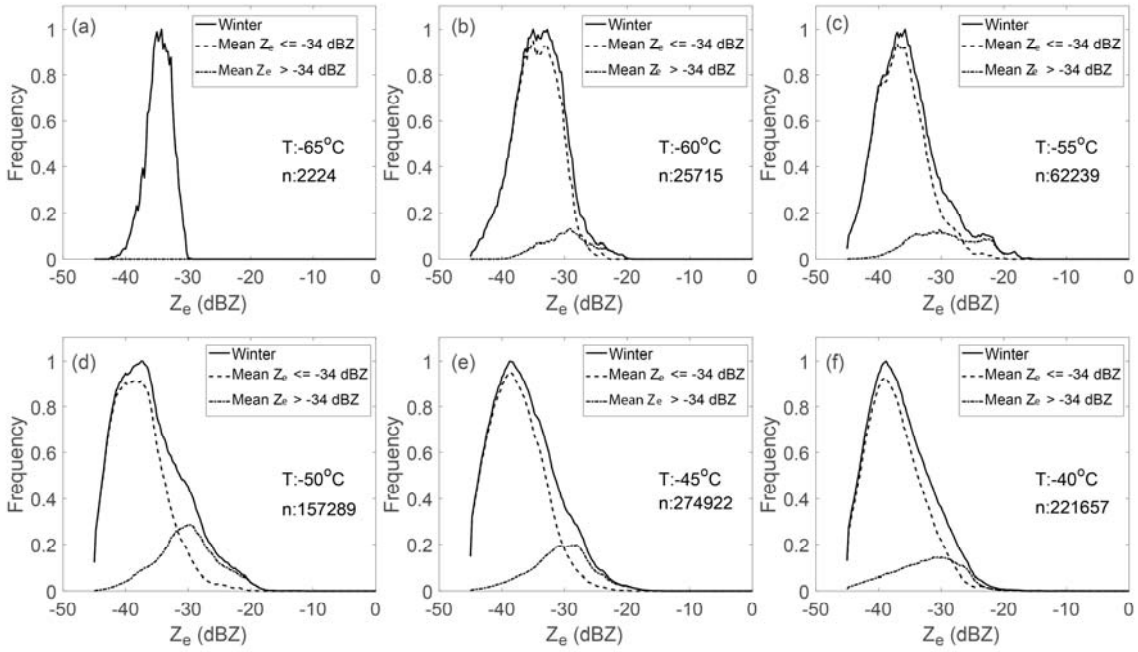

Figure 11. As in Fig. 8 but for winter.

6. Summary and discussion

Ice clouds are an important component of the planetary radiation budget and remain an uncertainty source in GCMs. This study used four years of vertically pointing Ka-band radar measurements at Beijing to characterize the physical and optical properties of ice clouds and to investigate the origination type of cirrus cloud. The goal was to present the quantified properties of ice clouds over the subtropical monsoon zone, which can be represented in GCMs towards a better understanding of the relationships between temperature and radar reflectivity under different formation conditions in various monsoon climates.

Winter monsoon and summer monsoon prevail alternately over Beijing, resulting in four distinct seasons. Ice clouds in winter and summer show strikingly different features. The specific findings about the properties of ice clouds can be summarized as follows:

1. The occurrence frequency, height, temperature and mean reflectivity of ice clouds in winter are lower than in summer. The average occurrence frequency over Beijing is 14%, and it is 20% in summer but less than 10% in winter. The diurnal variation of the occurrence frequency is not obvious, indicating an insensitive response to solar heating.
2. The CTHs of ice clouds range within 5.5–12.9 km, and the difference between the maximum and minimum reaches 6 km in every season. The mean CTH in summer is 2.2 km higher than in winter. The CBHs range within 5–12.4 km, and the

difference in the mean CBH between summer and winter is 2.1 km. In total, 86% of ice clouds are above 7 km in summer, and 81% are above 7 km in winter. Statistically, in the four seasons, 68% of clusters have a depth of less than 0.5 km, 90% less than 1 km, and 96% less than 1.5 km.

3. The EXT ranges through orders of magnitude from low values of less than 0.1 km to over 2800 km. Summer has the minimum mean, median and trimmed mean EXT, whereas ice clouds in autumn have the maximum mean, median and trimmed mean EXT. Statistically, about 75% of ice clouds have an EXT less than 50 km and 87% less than 100 km. In addition, the mean COD in spring, summer, autumn and winter is 4.3, 6.1, 4.6 and 4.5, respectively.
4. The radar reflectivity of ice clouds are dependent on the height, temperature and CD. The reflectivity mostly varies between −35 and −10 dBZ, and the mean reflectivity in summer is 10 dBZ higher than in winter. More than 95% of ice bins are below the temperature of −15°C, and the mean temperature of ice cloud in winter is the lowest among the four seasons. It was found that there is a strong linear relationship between the mean reflectivity and the CD.
5. Cirrus cloud occurs more frequently at −45°C than at other temperatures over Beijing, and cirrus clouds in spring are the most frequent among the four seasons.

The PDFs of reflectivity for cirrus cloud with respect to various temperatures were also investigated. It was found that the PDFs in the four seasons illustrate striking differences. A preliminary analysis indicates that cirrus clouds with mean reflectivity lower than −34 dBZ are likely to be of the *in situ*-origin type. Most cirrus clouds are of the *in situ*-origin type in winter and autumn; the *in situ*-origin type cirrus clouds are more frequent than liquid-origin cirrus clouds in spring, while summer features more liquid-origin cirrus clouds. In our recent work (Huo et al. 2020), the cirrus clouds are separated into three types via cloud-base temperature to study their particle reflectivity and movements, since there are differences among previous studies in the knowledge of the temperature range of cirrus clouds. Besides seasonal variation, cirrus clouds with different cloud-base temperatures also have different microphysical characteristics. In future work, we intend to further investigate the formation mechanisms of cirrus clouds in Beijing, as well as in other areas, for the purposes of parameterization in GCMs and the development of a locally adaptive Z_e–IWC relationship.

Data availability

The MODIS product data were obtained from http://ladsweb.nascom.nasa.gov. The AHI data were obtained from https://www.eorc.jaxa.jp/ptree/index.html. The radar data used here are available by special request to the corresponding author (huojuan@mail.iap.ac.cn).

Author contributions

Juan Huo designed the study and carried it out. Yufang Tian, Congzheng Han, Xue Wu, Yongheng Bi, Daren Lyu, Shu Duan and Bo Liu prepared some of the datasets. Juan Huo prepared the manuscript with contributions from all co-authors.

Competing interests

The authors declare that they have no conflicts of interest.

Acknowledgments

This work was supported by the National Natural Science Foundation of China (grant 41775032). We appreciate the valuable suggestions and insightful instructions from the reviewers. Thanks also to the ECMWF-ERA5 and AHI science teams for sharing their product datasets. We also acknowledge our Ka-radar team for their maintenance service during long-term measurements that made our research possible.

References

Adhikari, L., Wang, Z. and Deng, M.: Seasonal variations of antarctic clouds observed by cloudsat and calipso satellites. J. Geophys. Res. Atmos., 117, doi:10.1029/2011JD016719, 2012.

American Meteorological Society, cited 2019: Cirrus. Glossary of Meteorology. Available online at http://glossary.ametsoc.org/wiki/ Cirrus.

Austin, R. T., Heymsfield, A. J. and Stephens, G. L.: Retrieval of ice and cloud microphysical parameters using the CloudSat millimeter-wave radar and temperature. J. Geophys. Res. Atmos., 114, doi: 10.1029/2008JD010049, 2009.

Boucher, O., Randall, D., Artaxo, P., Bretherton, C., Feingold, G., Forster, P., Kerminen, V., Kondo, Y., Liao, H., Lohmann, U., Rasch, P., Satheesh, S., Sherwood, S., Stevens, B. and Zhang, X. Y.: Clouds and aerosols, in climate change 2013: The physical science basis. Contribution of working group I to the fifth assessment report of the intergovernmental panel on climate change, edited by T. Stocker et al.,. Cambridge Univ. Press,Cambridge, United Kingdom and New York, NY, USA, 2013.

Cotton, R. J., Field, P. R., Ulanowski, Z., Kaye, P. H., Hirst, E., Greenaway, R. S., Crawford, I., Crosier, J. and Dorsey, J.: The effective density of small ice particles obtained from in situ aircraft observations of mid-latitude cirrus. Quarterly Q. J. Roy. Meteor. Soc., 139, 1923–1934, doi: 10.1002/qj.2058, 2013.

Delanoë, J. and Hogan, R. J.: A variational scheme for retrieving ice cloud properties from combined radar, lidar, and infrared radiometer. J. Geophys. Res. Atmos., 113, doi: 10.1029/2007jd009000, 2008.

Delanoë, J. and Hogan, R. J.: Combined CloudSat-CALIPSO-MODIS retrievals of the properties of ice clouds. J. Geophys. Res. Atmos., 115, doi: 10.1029/2009jd012346, 2010.

Deng, M., Mace, G. G., Wang, Z. and Berry, E.: CloudSat 2C-ICE product update with a new Ze parameterization in lidar-only region. J. Geophys. Res. Atmos., 120, 12198–12208, doi: 10.1002/2015jd023600, 2015.

Deng, M., Mace, G. G., Wang, Z. and Okamoto, H.: Tropical composition, cloud and climate coupling experiment validation for cirrus cloud profiling retrieval using CloudSat radar and CALIPSO Lidar. J. Geophys. Res., 115, doi:10.1029/2009JD013104, 2010.

Dolinar, E. K., Dong, X., Xi, B., Jiang, J. H., Loeb, N. G., Campbell, J. R. and Su, H.: A global record of single-layered ice cloud properties and associated radiative heating rate profiles from an A-train perspective. Clim. Dynam., 53, 3069–3088, doi: 10.1007/s00382-019-04682-8, 2019.

Ge, J., Wang, Z., Liu, Y., Su, J., Wang, C. and Dong, Z.: Linkages between mid-latitude cirrus cloud properties and large-scale meteorology at the SACOL site. Clim. Dynam., 53, 5035–5046, https://doi.org/10.1007/s00382-019-04843-9, 2019.

Gultepe, I. and Heymsfield, A. J.: Introduction ice fog, ice clouds, and remote sensing. Pure Appl. Geophys., 173, 2977–2982, doi: 10.1007/s00024-016-1380-2, 2016.

Hahn, C. J. and Warren, S. G.: A gridded climatology of clouds over land (1971–96) and ocean (1954–97) from surface observations worldwide. Numeric Data Product NDP-026E, Carbon Dioxide Information Analysis Center, Oak Ridge National Laboratory, Oak Ridge, 2007.

Heymsfield, A., Bansemer, A., Wood, N. B., Liu, G., Tanelli, S., Sy, O. O., Poellot, M. and Liu, C.: Toward improving ice water content and snow-rate retrievals from radars. Part II: Results from three wavelength radar–collocated in situ measurements and CloudSat–GPM–TRMM radar data. J. Appl. Meteorol. Climatol., 57, 365–389, doi: 10.1175/jamc-d-17-0164.1, 2018.

Heymsfield, A., Schmitt, C. and Bansemer, A.: Ice cloud particle size distributions and pressure-dependent terminal velocities from in situ observations at temperatures from 0º to 86ºC. J. Atmos. Sci., 70, 4123–4154, doi:10.1175/JAS-D-12-0124.1, 2013.

Heymsfield, A. J., Krämer, M., Luebke, A., Brown, P., Cziczo, D. J., Franklin, C., Lawson, P., Lohmann, U., McFarquhar, G., Ulanowski, Z. and Tricht, K. V.: Cirrus clouds. Meteorological Monographs, 58, doi: 10.1175/amsmonographs-d-16-0010.1, 2017.

Heymsfield, A. J., Protat, A., Bouniol, D., Austin, R. T., Hogan, R. J., Delanoë, J., Okamoto, H., Sato, K., Zadelhoff, G.-J., Donovan, D. P. and Wang, Z.: Testing iwc retrieval methods using radar and ancillary measurements with in situ data. J. Appl. Meteorol. Climatol., 47, 135–163, doi: 10.1175/2007jamc1606.1, 2008.

Hogan, R. J., Mittermaier, M. P. and Illingworth, A. J.: The retrieval of ice water content from radar reflectivity factor and temperature and its use in evaluating a mesoscale model. J. Appl. Meteorol. Climatol., 45, 301–317, doi: 10.1175/jam2340.1, 2006.

Hong, Y. and Liu, G.: The characteristics of ice cloud properties derived from CloudSat and CALIPSO measurements. J. Climate, 28, 3880–3901, doi: 10.1175/jcli-d-14-00666.1, 2015.

Huo, J., Bi, Y., Lu, D. and Duan, S.: Cloud classification and distribution of cloud types in Beijing using Ka band radar data. Adv. Atmos. Sci., 36, 1–11, https://doi.org/10.1007/s00376-019-8272-1, 2019.

Huo, J., Han, C., Duan, M., Wu, X., Bi, Y. and Tian, Y.: Particle reflectivity and movements in cirrus clouds over Beijing from four years of Ka radar measurements. Atmos. Res., 105211, https://doi.org/10.1016/j.atmosres.2020.105211, 2020.

Jensen, E. J., Toon, O. B., Selkirk, H. B., Spinhirne, J. D. and Schoeberl, M. R.: On the formation and persistence of

subvisible cirrus clouds near the tropical tropopause. J. Geophys. Res. Atmos., 101, 21361–21375, doi: 10.1029/95jd03575, 1996.

Joos, H., Spichtinger, P., Reutter, P. and Fusina, F.: Influence of heterogeneous freezing on the microphysical and radiative properties of orographic cirrus clouds. Atmos. Chem. Phys.,, 6835–6852, doi:10.5194/acp-14-6835-2014, 2014.

Kanji, Z. A., Ladino, L. A., Wex, H., Boose, Y., Burkert-Kohn, M., Cziczo, D. J. and Krämer, M.: Overview of ice nucleating particles. Meteorological Monographs, 58, doi: 10.1175/amsmonographs-d-16-0006.1, 2017.

Kärcher, B.: Formation and radiative forcing of contrail cirrus. Nat. Commun., 9, 1824, doi: 10.1038/s41467-018-04068-0, 2018.

Kawamoto, K., Nakajima, T. and Nakajima, T. Y.: A global determination of cloud microphysics with AVHRR remote sensing. J. Climate, 14, 2054-2068, doi: 10.1175/1520-0442(2001)014<2054:Agdocm>2.0.Co;2, 2001.

Kienast-Sjögren, E., Rolf, C., Seifert, P., Krieger, U. K. and Peter, T.: Radiative properties of mid-latitude cirrus clouds derived by automatic evaluation of lidar measurements. Atmos. Chem. Phys., 16, 1–31, 2016.

Kollias, P., Clothiaux, E. E., Miller, M. A., Albrecht, B. A., Stephens, G. L. and Ackerman, T. P.: Millimeter-wavelength radars: New frontier in atmospheric cloud and precipitation research. B. Am. Meteorol. Soc., 88(10), 1608–1624, doi: 10.1175/bams-88-10-1608, 2007.

Kox, S., Bugliaro, L. and Ostler, A.: Retrieval of cirrus cloud optical thickness and top altitude from geostationary remote sensing. Atmos. Meas. Tech., 7, 3233–3246, doi: 10.5194/amt-7-3233-2014, 2014.

Krämer, M., Rolf, C., Luebke, A., Afchine, A., Spelten, N., Costa, A., Meyer, J., Zöger, M., Smith, J., Herman, R. L., Buchholz, B., Ebert, V., Baumgardner, D., Borrmann, S., Klingebiel, M. and Avallone, L.: A microphysics guide to cirrus clouds – part 1: Cirrus types. Atmos. Chem. Phys., 16, 3463–3483, doi:10.5194/acp-16-3463-2016, 2016.

Lawson, R. P., Woods, S., Jensen, E., Erfani, E., Gurganus, C., Gallagher, M., Connolly, P., Whiteway, J., Baran, A. J., May, P., Heymsfield, A., Schmitt, C. G., McFarquhar, G., Um, J., Protat, A., Bailey, M., Lance, S., Muehlbauer, A., Stith, J., Korolev, A., Toon, O. B. and Krämer, M.: A review of ice particle shapes in cirrus formed in situ and in anvils. J. Geophys. Res. Atmos., 124, 10049–10090, https://doi.org/10.1029/2018JD030122, 2019.

Liu, C.-L. and Illingworth, A. J.: Toward more accurate retrievals of ice water content from radar measurements of clouds. J. Appl. Meteorol., 39, 1130–1146, doi: 10.1175/1520-0450(2000)039<1130:Tmaroi>2.0.Co;2, 2000.

Luebke, A. E., Afchine, A., Costa, A., Grooß, J. U., Meyer, J., Rolf, C., Spelten, N., Avallone, L. M., Baumgardner, D. and Krämer, M.: The origin of midlatitude ice clouds and the resulting influence on their microphysical properties. Atmos. Chem. Phys., 16, 5793–5809, doi: 10.5194/acp-16-5793-2016, 2016.

Mace, G., Benson, S. and Vernon, E.: Cirrus clouds and the large-scale atmospheric state: Relationships revealed by six years of ground-based data. J. Climate Appl. Meteor., 19, 3257–3278, doi:10.1175/JCLI3786.1, 2006.

Matrosov, S. Y. and Heymsfield, A. J.: Empirical relations between size parameters of ice hydrometeor populations and radar reflectivity. J. Appl. Meteorol. Climatol., 56, 2479–2488, doi: 10.1175/jamc-d-17-0076.1, 2017.

Muhlbauer, A., Ackerman, T. P., Comstock, J. M., Diskin, G. S., Evans, S. M., Lawson, R. P. and Marchand, R. T.: Impact of

large-scale dynamics on the microphysical properties of midlatitude cirrus. J. Geophys. Res. Atmos., 119, 3976–3996, doi:10.1002/2013JD020035, 2014.

Nakajima, T. Y. and Nakajma, T.: Wide-area determination of cloud microphysical properties from noaa avhrr measurements for fire and astex regions. J. Atmos. Sci., 52, 4043–4059, doi: 10.1175/1520-0469(1995)052<4043:Wadocm>2.0.Co;2, 1995.

Pokharel, B. and Vali, G.: Evaluation of collocated measurements of radar reflectivity and particle sizes in ice clouds: J. Appl. Meteorol. Climatol., 50, 2104-2119, 2011.

Runheng, H. and Liou, K.-N.: Effects of horizontal orientation on the radiative properties of ice clouds.Adv. Atmos. Sci., 2, 20–27, doi: 10.1007/BF03179733, 1985.

Sassen, K., Wang, Z. and Liu, D.: Global distribution of cirrus clouds from CloudSat/Cloud-Aerosol Lidar and Infrared Pathfinder Satellite Observations (CALIPSO) measurements. J. Geophys. Res., 113, doi:10.1029/2008JD009972, 2008.

Sassen, K., Wang, Z. and Liu, D.: Cirrus clouds and deep convection in the tropics: Insights from CALIPSO and CloudSat. J. Geophys. Res. Atmos., 114, D00H06, doi:10.1029/2009JD011916, 2009.

Stubenrauch, C. J., Chedin, A., Radel, G., Scott, N. A. and Serrar, S.: Cloud properties and their seasonal and diurnal variability from TOVS path-B. J. Climate, 19, 5531–5553, doi: 10.1175/JCLI3929.1, 2006.

Wang, Z. and Sassen, K.: Cirrus cloud microphysical property retrieval using lidar and radar measurements. Part I: Algorithm description and comparison with in situ data. J. Appl. Meteorol., 41, 218–229, https://doi.org/10.1175/1520-0450(2002)041%3C0218:CCMPRU%3E2.0.CO;2, 2001a.

Wang, Z. and Sassen, K.: Cloud type and macrophysical property retrieval using multiple remote sensors. J. Appl. Meteorol., 40, 1665-1682, doi: 10.1175/1520-0450(2001)040<1665:Ctampr>2.0.Co;2, 2001b.

Wu, D. L., Austin, R. T., Deng, M., Durden, S. L., Heymsfield, A. J., Jiang, J. H., Lambert, A., Li, J.-L., Livesey, N. J., McFarquhar, G. M., Pittman, J. V., Stephens, G. L., Tanelli, S., Vane, D. G. and Waliser, D. E.: Comparisons of global cloud ice from MLS, CloudSat, and correlative data sets. J. Geophys. Res. Atmos., 114, doi: 10.1029/2008jd009946, 2009.

Wolf, V., Kuhn, T., Milz, M., Voelger, P., Krämer, M. and Rolf, C.: Arctic ice clouds over northern Sweden: Microphysical properties studied with the balloon-borne ice cloud particle imager B-ICI. Atmos. Chem. Phys., 18, 17371–17386, doi: 10.5194/acp-18-17371-2018, 2018.

Yang, P., K. N. Liou, L. Bi, C. Liu, B. Yi and Baum, B. A.: On the radiative properties of ice clouds: Light scattering, remote sensing, and radiation parameterization. Adv. Atmos. Sci., 32, 32–63, https://doi.org/10.1007/s00376-014-0011-z, 2015.

Yang, P. and Qiang Fu: Dependence of ice crystal optical properties on particle aspect ratio. J. Quant. Spectrosc. Ra., 110, 1604–1614, https://doi.org/10.1016/j.jqsrt.2009.03.004, 2009.

Zelinka, M. D., Klein, S. A. and Hartmann, D. L.: Computing and partitioning cloud feedbacks using cloud property histograms. Part I: Cloud radiative kernels. J. Climate, 25, 3715–3735, 2012.